PERGAMON

Applied Geochemistry 17 (2002) 825–836

Applied Geochemistry

www.elsevier.com/locate/apgeochem

Tracer and radionuclide sorption to vitric tuffs of Busted Butte, Nevada

H.J. Turin*, A.R. Groffman, L.E. Wolfsberg, J.L. Roach, B.A. Strietelmeier

Los Alamos National Laboratory, Los Alamos, NM 87545, USA

Received 23 January 2001; accepted 15 October 2001

Editorial handling by M. Gascoyne

Abstract

Field-scale unsaturated-zone tracer tests have been performed at Busted Butte, Nevada, near the potential high-level radioactive waste repository at Yucca Mountain. These tests are intended to improve our understanding of unsaturated-zone transport processes, and to test our ability to predict field-scale behavior using laboratory-scale measurements. The field tests use a mixture of nonreactive and reactive tracers. Nonreactive tracers include Br^-, I^-, 5 different fluorobenzoic acids, Na fluorescein, and a pyridone derivative. Reactive tracers include the metals Li, Mn, Co, and Ni, and the organic dye rhodamine WT. Rock samples from 3 different stratigraphic units at the Busted Butte test facility have been extensively characterized lithologically and mineralogically, and analyzed for Fe and Mn oxide content. Sorption of Np, Pu, Am and the field tracers onto these 3 rocks has been measured using batch techniques. Results confirm that the nonreactive tracers are indeed nonreactive, and show that sorption of radionuclides and sorbing tracers increases with increasing degree of rock alteration, as evidenced by increasing levels of smectite and Fe and Mn oxides. Among the radionuclides, Am and Pu sorb much more strongly than Np; the tracers' degree of sorption is rhodamine WT=Li $\ll$ Mn $<$ Ni $<$ Co. Pu, Co, Mn, Ni and rhodamine WT exhibits strongly nonlinear sorption; Mn and Ni behavior may reflect competition with Co for sorption sites.

1. Introduction

The vitric tuffs of Busted Butte, Nevada, are stratigraphically correlative and mineralogically similar to unsaturated rocks between the potential high-level nuclear waste repository at Yucca Mountain and the underlying water table. This unsaturated zone, together with the engineered barrier system within the repository itself, and the saturated zone below, comprise a multiple-barrier defense against radionuclide transport to the accessible environment. The future behavior of the entire system is being predicted using a series of complex conceptual and numerical models. Field-scale tracer transport experiments have been conducted at Busted Butte (Bussod et al., 1998) and at the C-Wells (Reimus et al., 1998, 1999) to help validate the use of these models for the unsaturated-zone and saturated-zone geologic barriers, respectively.

Unsaturated-zone tracer tests have been conducted at Busted Butte, approximately 8 km SE of Yucca Mountain. The stratigraphic setting of the tests includes the lower Topopah Springs and upper Calico Hills Tuffs, rocks that lay between the potential repository horizon within the Topopah Springs Tuff and the water table. Faulting has lifted these rocks from an inaccessible depth beneath Yucca Mountain to the surface at Busted Butte. The goal of tracer tests has been to increase our understanding of unsaturated-zone flow and transport processes, and specifically to test our ability to predict field-scale reactive transport using laboratory-scale hydraulic and sorption measurements. The Busted Butte facility consists of a 74-m main adit and a perpendicular 16.5-m experimental alcove, blasted into the side of the

* Corresponding author. Fax: +1-505-665-6339.
E-mail address: turin@lanl.gov (H.J. Turin).

0883-2927/02/$ - see front matter
PII: S0883-2927(02)00042-2

butte. Numerous horizontal boreholes drilled from the adit and alcove into bedrock enable injection of tracer, collection of porewater and rock samples, and geophysical monitoring of the tests. The facility and the tests performed there are described in detail by Bussod et al. (1998).

Predictions of field-scale radionuclide transport rely on laboratory-scale sorption measurements (Triay et al., 1997). These predictions cannot be vaildated by conducting field experiments using radioactive materials. The task is to select a suite of nonradioactive surrogate tracers with a range of sorption properties similar to those of radionuclides of concern, measure tracer properties in the laboratory, predict field-scale transport using those measurements, and then compare those predictions to actual field-scale tracer behavior. In this paper, the results of the first steps of this process are presented, including a selection of surrogate tracers, laboratory-scale measurement of radionuclide and tracer sorption, and a comparison of radionuclide and tracer behavior. Results of the field experiment continue to be analyzed, and will be discussed in future publications.

2. Tracer selection

The tracer selection process involved a series of compromises between competing factors, including desirable geochemical properties, regulatory acceptability, health and safety concerns, analytical ease, and cost. Selecting reactive tracers that exhibit significant sorption yet move rapidly enough to be detected within a reasonable experimental time frame is particularly challenging. The tracers finally selected for the Busted Butte field experiments include nonreactive anionic tracers with a range of diffusivities, metal tracers displaying a range of reactivity, and organic dyes with a variety of characteristics. After tracers have been selected, injection concentrations must be determined. While low concentrations minimize the geochemical alteration of the system, minimize regulatory hurdles, and minimize tracer costs, higher concentrations enable earlier breakthrough detection and may decrease analytical expenses.

Nonreactive tracers used in the field experiments have included Br^-, I^-, 5 different fluorinated benzoic acids (FBAs), Na fluorescein (uranine, acid yellow 73), and carbomoyl-2(1H)-pyridone (henceforth, ''pyridone''). Bromide was used in all the injection boreholes since testing was initiated; it has a relatively low molecular weight (high diffusivity), low cost, and excellent analytical properties. Iodide has similar properties to Br^-, and was introduced approximately 1 year into the experiment, after the system approached a hydraulic steady state. By comparing Br^- and I^- field behavior, it was possible to assess the impact of the strong hydraulic transients produced by the initiation of tracer injection. The FBAs include 2,4-difluorobenzoic acid (2,4-diFBA), 2,6-difluorobenzoic acid (2,6-diFBA), 2,4,5-trifluorobenzoic acid (2,4,5-triFBA), 2,3,4,5-tetrafluorobenzoic acid (2,3,4,5-tetraFBA), and pentafluorobenzoic acid (PFBA; see Atkinson and Bukowiecki, 2000; Farnham et al., 2000 and references therein). Compared to the halides, the FBAs have higher molecular weights and lower diffusivities, higher costs, and are subject to more analytical interference. At the pH of the field and laboratory experiments, the FBAs occur as fluorobenzoate anions. The number of FBAs available makes them valuable for ''tagging'' individual injection boreholes. Each of the injection boreholes was tagged with a single FBA; FBA analyses enabled the determination of the extent of mixing between the different tracer plumes and the estimated transverse dispersion. Sodium fluorescein and ''pyridone'' are organic dye tracers. Sodium fluorescein's strong fluorescence under ultraviolet illumination enables qualitative determination of breakthrough during sample collection at the field site, but its susceptibility to photodegradation and the sensitivity of its fluorescence to matrix variations limit its usefulness as a quantitative tracer. ''Pyridone'' is an experimental tracer (Nelson et al., 1989) that has been used by the US Geological Survey for saturated-zone tracer testing at the C-Wells (Geldon et al., 1997), and was added to the Busted Butte tracer mixture to further evaluate its usefulness for future field studies.

Reactive metal tracers include Li, Mn, Co, Ni, Ce and Sm. Lithium is a weakly sorbing tracer whose value has been demonstrated in saturated-zone tracer tests at the Yucca Mountain C-Wells complex (Reimus et al., 1998, 1999). Lithium is quite soluble, and the breakthrough concentrations at the collection boreholes are readily analyzed. The transition metals Mn, Co, and Ni sorb more strongly than Li, and are far less soluble. Therefore, breakthrough concentrations are lower, leading to analytical difficulties. In particular, varying matrix effects lead to increased uncertainty in the inductively coupled plasma–mass spectrometry (ICP–MS) analyses of transition metals at the ppb level. Furthermore, Mn, unlike the other metals, has a significant background level that may interfere with breakthrough detection. Previous tracer tests using transition metals are rare, although Co and Ni were injected in a saturated-zone test near Munich (Müller, 2000). The rare-earth metals Sm and Ce were also added to the tracer mixture at Busted Butte. These metals have very low solubilities under field conditions, and it is likely that they precipitated within the tracer tanks (Kearney et al., 2000). Additional metal tracers that were considered for the Busted Butte experiment include Mo (as molybdate) and Re (as perrhenate); preliminary laboratory studies revealed no significant tracer/rock interaction and both tracers were eliminated from further consideration.

Rhodamine WT (acid red 388) was also added to the Busted Butte tracer mixture. This intensely colored organic dye is known to sorb to rock and soil materials (Sabatini and Austin, 1991; Kasnavia et al., 1999), and was used primarily to help locate tracer plumes in rock samples collected during post-test excavation.

3. Laboratory sorption studies

The sorption of 3 radionuclides of concern (Np, Am and Pu) onto the 3 distinct rock units involved in the Busted Butte field tests were measured, for comparison to the reactive tracer results and for comparison with other Yucca Mountain data on radionuclide sorption. The sorption properties of the entire suite of Busted Butte tracers were also measured, to verify the non-reactivity of the supposedly nonreactive tracers and to determine the sorption characteristics of the reactive tracers. These sorption characteristics, expressed in terms of sorption isotherm parameters, were used for numerical modeling predictions of field-scale transport of the reactive tracers. The tracer and radionuclide sorption tests were performed by different teams, using slightly different standard procedures. Material preparation and detailed procedures for the tests are described below.

3.1. Rock samples

The Busted Butte facility encompasses 3 different stratigraphic horizons: two subunits of the Topopah Springs vitrophyre, and the Calico Hills Tuff. These 3 horizons are referred to as Tptpv2, Tptpv1, and Tac, respectively. A sample of each horizon was selected from cores collected during borehole drilling. The samples were crushed and sieved to remove particles > 500 μm; the fines fraction was retained. In addition to the sorption measurements, the three rocks were analyzed for mineral content by quantitative X-ray diffraction (QXRD), for free Fe oxides by the citrate-dithionite method (Loeppert and Inskeep, 1996) and for Mn oxides by the hydroxylamine method (Gambrell, 1996). Detailed lithologic descriptions of the rocks are presented in Table 1; QXRD and Fe and Mn oxide analysis results are presented in Table 2. These analyses show that all 3 rocks consist primarily of amorphous volcanic glass (ranging from 61 to 94%), and that the rocks have been altered to varying degrees, as revealed by differing contents of smectite, Fe oxides and Mn oxides.

3.2. Synthetic Busted Butte porewater

To minimize mineral dissolution and precipitation reactions in the field experiment, the tracer solutions were mixed in a synthetic porewater designed to mimic the in-situ porewater major-ion chemistry. The in-situ chemistry was determined by analyzing porewater extracted by centrifugation from 3 Tac rock samples at Busted Butte. The resulting analysis (Table 3) shows that the porewater is a mixed-ion (Ca–Na–HCO_3–SO_4) water with a total dissolved solid (TDS) of approximately 200 mg/l and a high dissolved Si concentration

Table 1
Lithologic descriptions

Stratigraphic horizon (Yucca Mountain sample identifier)	Lithologic Description
Topopah Springs Tuff, Tptpv2 (UZTT-BB-PH1–7)	Moderately welded vitric tuff containing 25% pumice lapilli 1–30 mm long, flattened and aligned with the bedding/compaction direction. The rock also contains 25% glass shards 0.1–10 mm, 1–2% cryptocrystalline lithic grains, and 1–2% feldspar and minor biotite phenocrysts. The remainder of the rock (45–50%) is fine ash particles <0.1 mm. There is minor argillic and very slight hematitic alteration.
Topopah Springs Tuff, Tptpv1 (UZTT-BB-PH1–3)	Vitric nonwelded tuff composed predominantly of undeformed pumice clasts, round to elongate, 1–25 mm (50%). Some of the pumice clasts are aligned with the bedding. Other clasts include cryptocrystalline lithic grains 1–22 mm (3–5%) and traces of feldspar and biotite phenocrysts <1 mm. The remainder of the rock is composed of vitric ash particles <1 mm.
Calico Hills Tuff, Tac(UZTT-BB-PH1–4)	Vitric nonwelded pumice-lapilli tuff containing 75% pumice clasts 0.1–15 mm, mostly vitric but with local clayey alteration and rare patches of possible secondary Mn minerals. Other constituents include 15–20% phenocrysts <1 mm, of feldspar quartz, and biotite, 3–5% cryptocrystalline lithic grains <1 mm, and 1% glass chunks <1 mm.

Table 2
Quantitative X-ray diffraction, Fe and Mn oxide analysis results

	Tptpv2	Tptpv1	Tac
Smectite (%)	8±2	nd[a]	18±5
Kaolinite (%)	2±1	nd	nd
Mica (%)	Trace	Trace	Trace
Quartz (%)	1±1	1±1	6±1
Opal-C (%)	nd	1±1?	nd
Cristobalite (%)	nd	nd	1±1
Calcite (%)	nd	nd	Trace?
Hematite (%)	nd	nd	1±1
Feldspar (%)	3±1	4±1	12±2
Unidentified (%)	nd	nd	1±1
Amorphous (%)	86±3	94±2	61±6
Free Fe oxides (ppm Fe)	1000±4.3	300±21	1200±29
Mn oxides (ppm Mn)	37±5.3	7.9±2.4	130±3.9

Uncertainty listed is estimated 2σ error for QXRD analyses, one standard deviation for Fe and Mn oxide analyses.
[a] nd, not detected.

Table 3
Busted Butte porewater and tracer mixture compositions

Constituent	Busted Butte porewater (measured; mg/l)	Tracer mixture (calculated; mg/l)
Br	0.1	920
Ca	21.8	22
Ce	<0.6	1.9
Cl	17.8	30
Co	<1.1	2.5
F	1.7	1.7
Fe	<0.2	<0.2
HCO_3 (est)	46.3	43
I	Not analyzed	380
K	3.4	120
Li	0.1	80
Mg	3.7	3.7
Mn	<0.6	2.8
Na	19.6	21
Ni	<1.0	2.5
NO_3	23.4	23
PO_4	<0.2	<0.2
Si	32.3	32
Sm	<0.6	2.1
SO_4	31.7	32
Sr	0.4	0.4
Fluorescein anion	0	8.8
2,4,5-triFBA	0	100
Approximate TDS	200	1830
Ionic strength (mmol)	3.4	19

(~32 mg/kg Si). The synthetic porewater used in the field experiments consists of appropriate inorganic salts dissolved in deionized groundwater collected from a local well. The deionization process leaves the naturally high Si concentration intact, thus alleviating the difficulties of Si dissolution. The resulting synthetic porewater closely resembled the in-situ porewater in every major respect. The synthetic Busted Butte water ("BBW") used for the laboratory sorption experiments was prepared similarly, but without the high dissolved Si concentration.

3.3. Radionuclide solutions

Separate radionuclide solutions were prepared for the 3 actinides studied, ^{237}Np(V), ^{239}Pu(V), and ^{243}Am(III). In each case, a concentrated acidified stock solution was prepared and immediately diluted in BBW to produce 5 different concentrations, ranging from near the solubility limit down to the detection limit (Np: 10^{-5}–7×10^{-7} *M*; Pu: 10^{-6}–10^{-8} *M*; Am: 5×10^{-9}–5×10^{-10} *M*). Solution pH was not adjusted, and was measured at 7.7 for Am and Pu, and 8.1–8.2 for Np. The Pu oxidation state of the stock solution was determined by ultraviolet/visible spectroscopy; the oxidation state of the diluted solutions cannot be measured directly, but the authors believe that Pu(V) is stable in the dilute solutions. Redox reactions may affect Pu sorption, as discussed below.

3.4. Tracer solutions

Two different tracer mixtures were prepared. The first consisted of the full suite of halides, dyes, metals, and a single FBA (2,4,5-triFBA), dissolved at full field strength in BBW (Table 4). Table 3 compares the calculated composition of the field-strength tracer mixture to the in-situ porewater composition, and demonstrates that the high tracer concentrations needed to assure early tracer detection completely dominate the solution chemistry, increasing TDS and ionic strength by factors of 9 and 5.5, respectively. A series of dilutions of this mixture in BBW resulted in 7 different concentrations, ranging down to 0.001 of the field strength. Each solution was adjusted to pH 7.0±0.2 by addition of 1 N NaOH. (The small amount of NaOH added would not significantly affect overall Na concentrations in the mixture.)

A second mixture, designed to confirm the non-reactive nature of the FBAs, consisted of all 5 FBAs dissolved in BBW at 100 mg/kg, and similarly adjusted to pH 7.0±0.2. Sorption of the FBA mixture was measured only at this single concentration level, while 2,4,5-triFBA sorption was measured over a range of concentrations as part of the full tracer mixture.

3.5. Radionuclide sorption procedure

Prior to addition of the radionuclide solution, the crushed tuff samples were equilibrated with the BBW synthetic porewater by shaking for 3 weeks, followed by

Table 4
Tracer mixture used for batch sorption experiment

1000 mg/kg LiBr (80 mg/kg Li^+, 920 mg/kg Br^-)
500 mg/kg KI (382 mg/kg I^-)
100 mg/kg 2,4,5-triFBA
10 mg/kg sodium fluorescein
10 mg/kg "pyridone"
10 mg/kg rhodamine WT
10 mg/kg $NiCl_2 \cdot 6H_2O$ (2.5 mg/kg Ni^{2+})
10 mg/kg $MnCl_2 \cdot 4H_2O$ (2.8 mg/kg Mn^{2+})
10 mg/kg $CoCl_2 \cdot 6H_2O$ (2.5 mg/kg Co^{2+})
5 mg/kg $SmCl_3 \cdot 6H_2O$ (2.1 mg/kg Sm^{3+})
5 mg/kg $CeCl_3 \cdot 7H_2O$ (1.9 mg/kg Ce^{3+})

centrifuging (2 h at 39,400 RCF) and decanting the solution. Tuff samples were mixed with the tracer solutions under a normal atmosphere in a ratio of approximately 1 g rock to 20 g solution, shaken for 3 weeks in polycarbonate centrifuge tubes, and again centrifuged (1 h at 39,400 RCF). The resulting supernatant was filtered (0.45 μm) and analyzed for radionuclide activity by liquid scintillation counting. The measured activities were converted to masses assuming 100% counting efficiency. Each combination of a given rock and a given tracer solution was run in duplicate. In addition to the rock samples, duplicate rock-free "controls" were run for each tracer solution, to monitor any losses not due to rock sorption, such as degradation, volatilization, or sorption onto labware.

3.6. Tracer sorption procedure

The tracer sorption procedure was similar to the radionuclide sorption procedure, with the exception of 1-week pretreatment and sorption periods and a ratio of 7 g rock to 30 g solution. Centrifugation for phase separation was 1 h at 32,600 RCF. Each rock/solution combination and each rock-free control was run in triplicate. Final solution concentrations were measured by ion chromatography (Br^-, I^-), high-pressure liquid chromatography (FBAs), spectrofluorimetry (dyes) and ICP–MS (metals).

3.7. Calculations

For both tracers and radionuclides, differences between the final solution concentrations and the control concentration were attributed to sorption. (Except for rhodamine WT and the highest concentrations of Mn, Ni, and Co, control concentrations were in excess of 90% of initial tracer concentration in virtually all cases. The loss of metals at high concentration may reflect precipitation, while the rhodamine WT data may reflect sorption to the plastic centrifuge tubes.) Equilibrium solution concentrations (C) and sorbed concentrations (S) were calculated and converted to μg solute (tracer or radionuclide)/g (rock or solution). For non-sorbing tracers, S varied around zero, with numerous negative values. For these tracers, an effective K_D was calculated by linear regression of the raw S and C values. For sorbing tracers and radionuclides, both S and C were log-transformed to maximize statistical validity (Bowman et al., 1984) before isotherm-fitting was attempted. The log-transformed data was fitted to both the Freundlich isotherm [Eq. (1)] and the linear isotherm [Eq. (2)] by varying the parameters (K_F, n, K_D) in the log-transformed isotherms to minimize the sum of squares of the differences between observed and calculated $\log(S)$ values.

$$S = K_F \cdot C^n$$
$$\log(S) = \log(K_F) + n \cdot \log(C) \quad (1)$$

$$S = K_D \cdot C$$
$$\log(S) = \log(K_D) + \log(C) \quad (2)$$

Because all solutions and standards were prepared on a mass basis (mg/kg), resulting isotherm parameters are expressed on a mass basis (e.g. g/g for K_D). The differences between these units and more familiar volumetric units (e.g. ml/g for K_D) are insignificant relative to uncertainties in the values; thus the units can be considered equivalent.

4. Results and discussion

4.1. Radionuclide sorption

Fitted isotherm parameters for radionuclides and sorbing tracers are presented in Tables 5 (Freundlich) and 6 (linear); observed radionuclide sorption data and fitted isotherms are presented in Fig. 1. Plutonium sorption was markedly nonlinear ($n = 0.74–0.95$), while Am and Np sorption was close to linear ($n = 1 \pm 0.1$). The results are consistent with previous reports of nonlinear Pu sorption and linear Np sorption to Yucca Mountain tuffs (Triay et al., 1997); Am sorption linearity has not previously been discussed. The divergence between the observed Pu data in Fig. 1 and the best-fit linear isotherms (dashed lines) shows that the linear K_D model cannot fully capture Pu sorption behavior. The Freundlich isotherm (solid lines), on the other hand, describes Pu sorption quite well. The nonlinear behavior of Pu may be attributable to redox reactions. At higher concentrations, disproportionation of Pu(V) leads to an increased proportion of strongly sorbing Pu(IV) and an increase in apparent sorption.

Presenting a K_D value for a nonlinearly sorbing material such as Pu is somewhat misleading, because the

Table 5
Freundlich isotherm parameters for radionuclides and sorbing tracers

		Tptpv2	Tptpv1	Tac
Np	K_F	1.0	0.37	1.4
	n	1.1	0.91	0.97
Pu	K_F	130	7.5	1700
	n	0.74	0.79	0.95
Am	K_F	310	140	260
	n	0.96	0.90	0.95
Li	K_F	0.93	0.37	1.3
	n	0.89	0.92	0.91
Mn	K_F	140	9.6	470
	n	1.1	0.88	1.3
Co	K_F	51	16	79
	n	0.55	0.59	0.57
Ni	K_F	260	14	1400
	n	0.91	0.71	1.1
Rhodamine WT	K_F	4.0	0.38	1.9
	n	1.5	1.5	1.3

K_F $(\mu g/g)^{(1-n)}$; n, dimensionless.

K_D value is a function of the experimental conditions (i.e. initial solution concentrations) in addition to the actual sorption behavior. Nevertheless, results of previous radionuclide sorption measurements for Yucca Mountain tuff have been used to produce a table of recommended K_D values for performance assessment use (Triay et al., 1997). In Table 6, the best-fit K_D values are compared with those recommended values. (Note that the authors' large K_D ranges for Pu are dominated by the systematic variability caused by fitting a linear model to nonlinear behavior rather than by experimental variability.)

Table 6 shows that the results for Am and Np sorption were quite similar to the project recommendations for unsaturated-zone vitric tuff (Triay et al., 1997). The best-fit Pu sorption K_D values, on the other hand, showed far more variability (18–2500 g/g) than the recommended range (50–200 ml/g). The observed sorption onto Tptpv1 was lower than the recommended range, and sorption onto Tptpv2 and Tac was far higher. Triay et al. (1997) note that Pu sorption can vary widely as a function of water and rock chemistry, and is particularly sensitive to redox conditions. Although the authors believe that Pu(V) is stable in the initial dilute aqueous solution, interactions with rock mineral phases during the course of the experiment may have altered the oxidation state of Pu and thus its sorption behavior. Unfortunately, Pu oxidation states cannot presently be determined in these dilute solutions, so this hypothesis cannot be directly tested. For all 3 radionuclides, Tac showed the highest degree of sorption and Tptpv1 the lowest. While the small data set does not warrant extensive statistical analysis, it is interesting to observe that Pu sorption is more highly correlated with smectite content ($r^2 = 0.99$) and Mn oxides (0.98) than with Fe oxides (0.81), while Np sorption is most strongly correlated with Fe oxides (1.00), and less correlated with either smectite (0.91) or Mn oxides (0.74). These results are consistent with previous observations of radionuclide sorption to individual mineral phases (Triay et

Table 6
Linear isotherm parameters for radionuclides and sorbing tracers

		Tptpv2	Tptpv1 (g/g)	Tac	Yucca Mountain literature (ml/g)
Np	K_D	1.1	0.3	1.4	1
	Range	1.1–1.4	0.3–0.5	1.2–1.5	0–15
Pu	K_D	960	18	2500	100
	Range	300–1700	10–30	1900–3100	50–200
Am	K_D	460	360	460	400
	Range	410–480	350–460	440–510	100–1000
Li	K_D	0.88	0.35	1.3	
	Range	0.45–1.3	0.21–0.64	0.67–1.8	
Mn	K_D	86	15	98	
	Range	5.9–110	3.2–18	4.0–130	
Co	K_D	910	120	1600	
	Range	230–2600	40–480	420–4500	
Ni	K_D	430	48	670	
	Range	50–540	20–90	60–870	
Rhodamine WT	K_D	1.7	0.39	1.1	
	Range	0.3–4.2	0.09–1.3	0.4–2.9	

Literature values are recommended values for unsaturated vitric tuff (Triay et al., 1997).

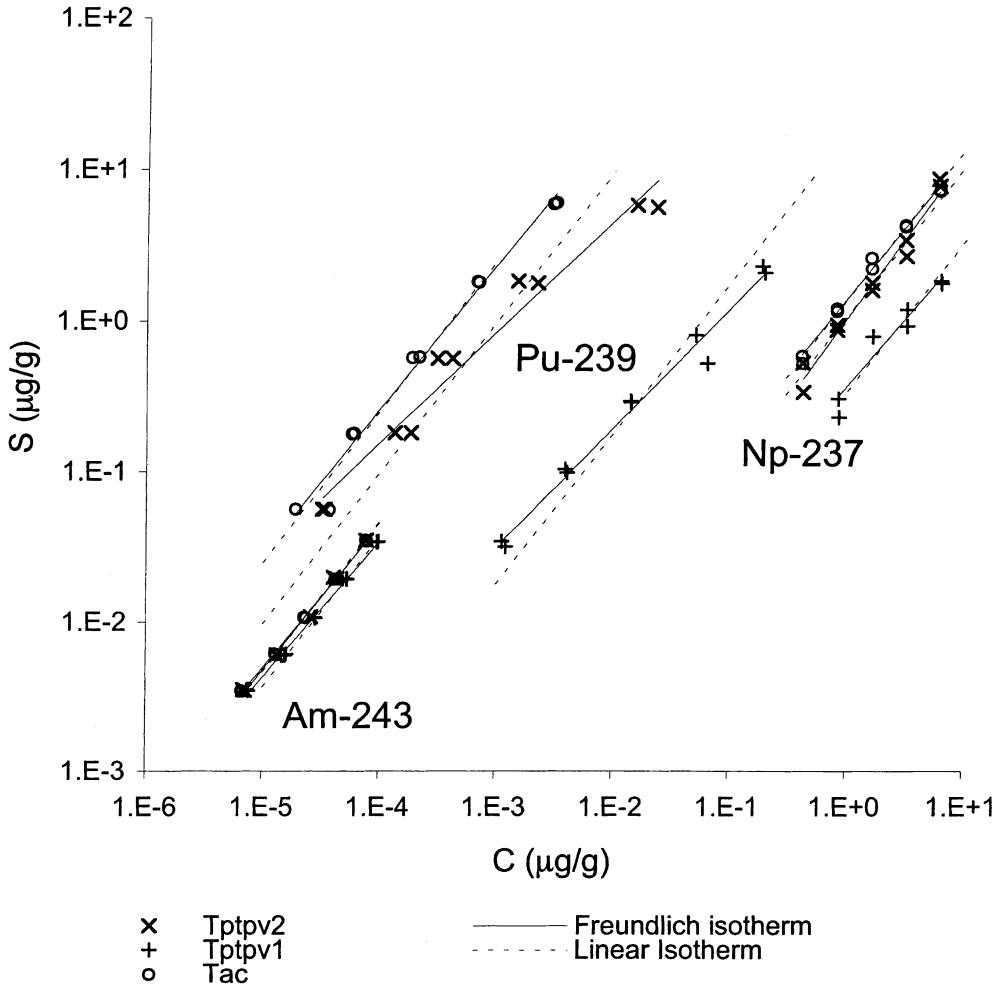

Fig. 1. Radionuclide batch sorption results.

al., 1997). While previous work with Am suggests that it is strongly sorbed to both Fe and Mn oxide surfaces and clays (Triay et al., 1997), the present results show strong correlation to Fe oxides (0.96) but much weaker correlation to smectite (0.69) and Mn oxides (0.47).

4.2. Nonsorbing tracers

The batch studies confirmed the nonsorbing behavior of Br^-, I^-, Na fluorescein, "pyridone," and the 5 FBAs. Results for the halides and dyes are presented in Fig. 2; and for the FBAs in Fig. 3. (Note that 2,4,5-triFBA sorption was measured over a range of concentrations, while sorption of the other FBAs was measured at a single concentration.) The observed scatter in the data is typical for non-sorbing species, in which S is calculated as a small difference between two large numbers (initial and final solution concentrations). The dashed lines on Figs. 2 and 3 show the predicted uncertainty in S values for a non-sorbing species, assuming a 5% uncertainty in measured C values. Almost all the observed data fall within this uncertainty range. In all cases, calculated K_D values were less than 0.1 g/g.

4.3. Sorbing tracers

Sorption of reactive metals is a very complex phenomenon, involving solution complexation, kinetics, ion exchange, and surface processes. Under the conditions of the batch sorption experiments, these complications are compounded by competition for sorption sites between the different tracers in the mixture, and between the tracers and the major ions in the synthetic porewater. The purpose of these experiments was not to elucidate the details of these processes, but rather to quantify to the extent possible the macroscopic sorption behavior of the different tracers using the actual field tracer mixture and actual field rocks.

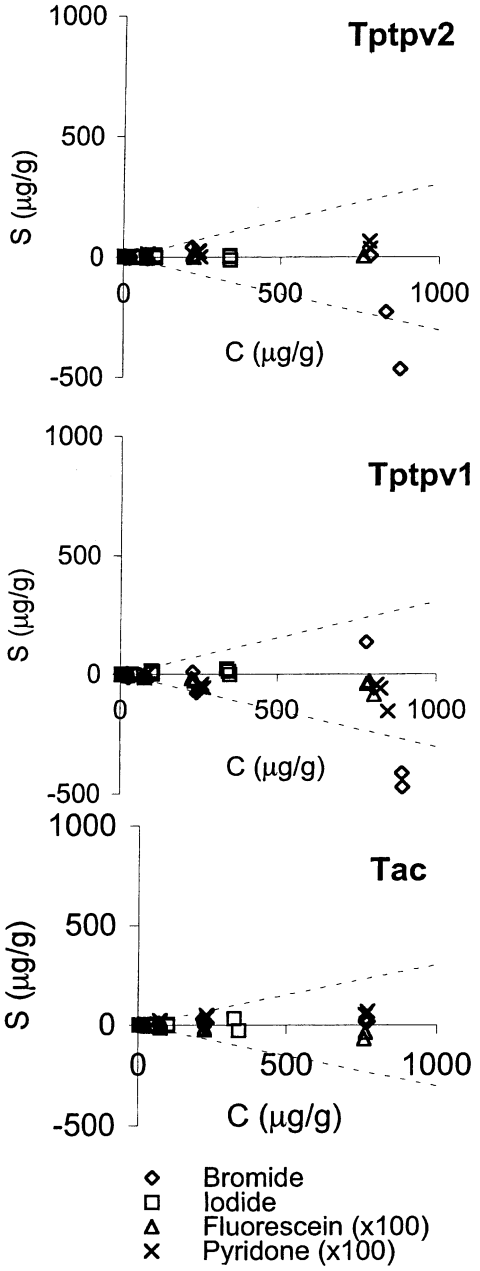

Fig. 2. Batch sorption results for nonreactive halides and dyes. Dashed lines show predicted uncertainty in S, assuming 5% analytical uncertainty for C.

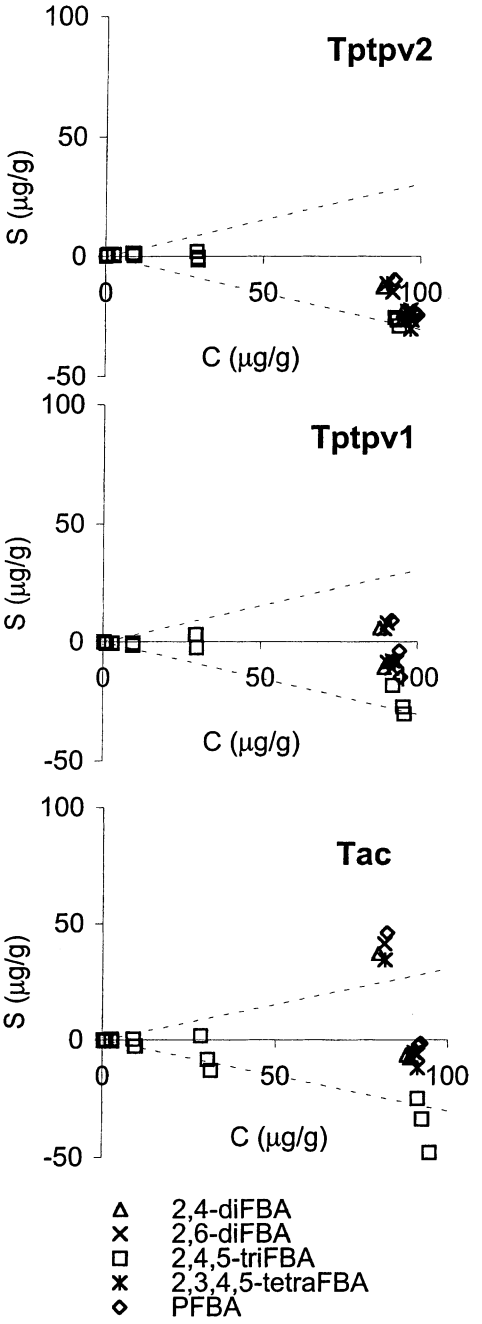

Fig. 3. Batch sorption results for fluorinated benzoic acids (FBAs). Dashed lines show predicted uncertainty in S assuming 5% uncertainty for C.

Sorption results for Li, Mn, Co, Ni, and rhodamine WT are presented in Fig. 4, together with fitted Freundlich and linear isotherms. Resulting isotherm parameters are presented in Tables 5 and 6. Although Sm and Ce were included in the tracer mixture for consistency with field procedures, precipitation reactions (Kearney et al., 2000) effectively removed them from solution and no meaningful sorption results were obtained.

Li sorption to the 3 rocks was slightly nonlinear ($n = 0.89-0.92$), but well described by the Freundlich isotherm (Fig. 4). Linearized K_D values ranged from

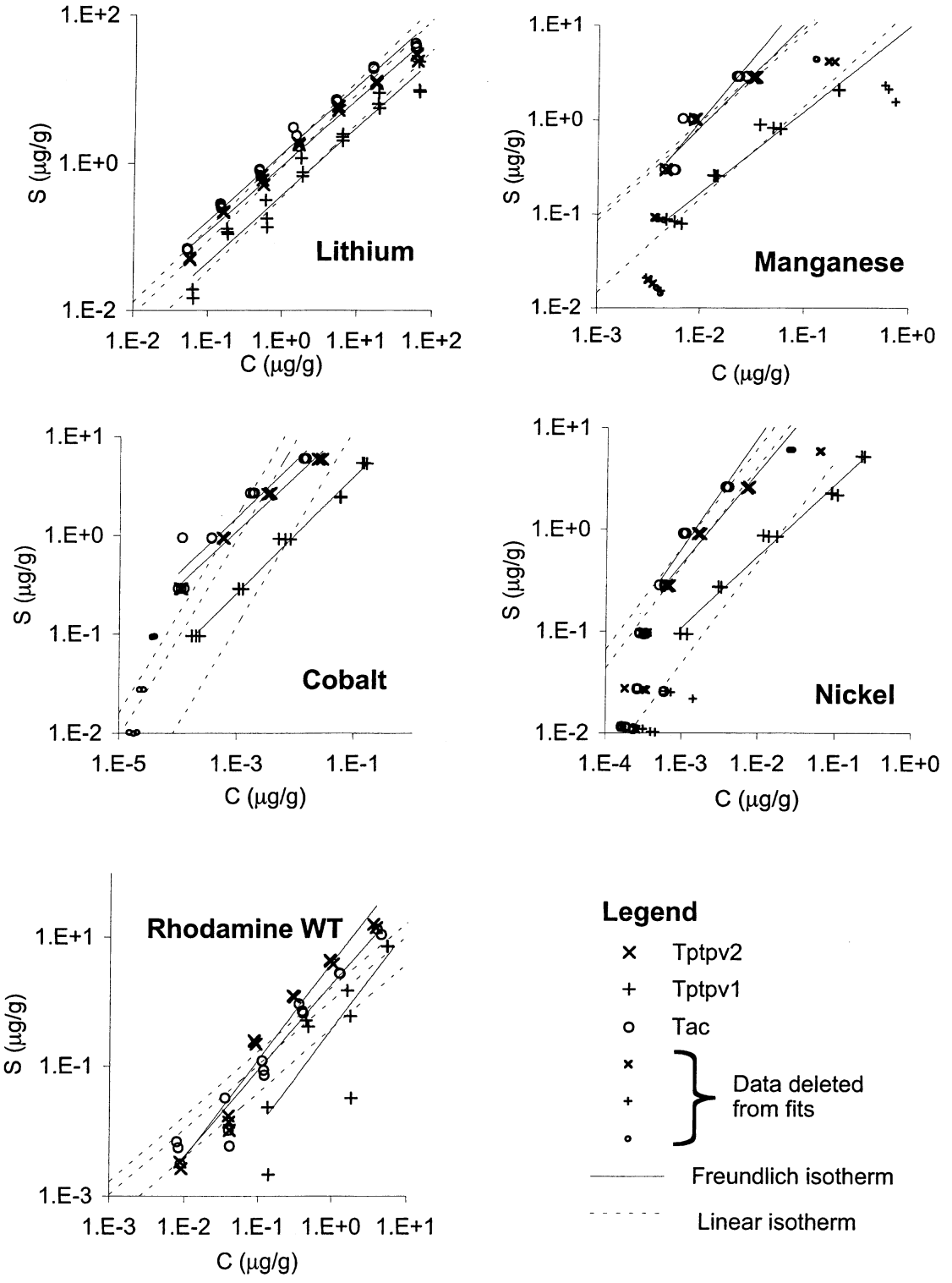

Fig. 4. Batch sorption results for reactive tracers.

0.35 to 1.3 g/g, and were well correlated with smectite content ($r^2 = 0.98$), extractable Fe (0.94) and extractable Mn (0.88). The observed Li sorption is significantly higher than would be predicted based purely on the rocks' smectite content (Anghel et al., 2002). This increased sorption may well be due to specific sorption of Li to Fe oxides, as cited by Schwertmann and Taylor (1989). Another possible complication, both in the laboratory and field studies, is competition for sorption sites between Li and the high K concentration in the tracer mixture.

The determination of Mn sorption was complicated by natural background levels of Mn in the tuff, potential precipitation of Mn at high solution concentrations, competition with other metals for sorption sites, and the intrinsic complexity of Mn chemistry in natural systems (Gambrell, 1996). These complications are reflected in the strongly nonlinear trend to the $S-C$ data plotted logarithmically (Fig. 4). This nonlinearity indicates that neither a Freundlich nor a linear isotherm model can adequately explain the observations. At low solution concentrations, the naturally occurring Mn becomes significant relative to the added tracer Mn. Calculations attribute this additional Mn to decreased sorption, resulting in an apparent downward curve at low concentrations (Fig. 4), and apparent negative sorption at the lowest concentrations (not shown in log–log space, Fig. 4). At high concentrations, decreased sorption relative to the Freundlich isotherm may reflect competition for limited sorption sites. Both Mn and Ni (see later) show this effect, suggesting that they are being displaced by the more strongly sorbing Co ions. In an attempt to quantify the "true" sorption, low-concentration and high-concentration points that strongly diverged from a linear trend (small symbols in Fig. 4) were ignored and the remaining points (large symbols) were fitted to Freundlich and linear isotherms. The arbitrariness of this procedure suggests that the resulting isotherm parameters should be considered highly uncertain. Despite this uncertainty, Mn sorption appears to follow the pattern of the other metals, with strongest sorption to the Tac and weakest to the Tptpv1. Best-fit K_D values ranged from 15 to 98 g/g, and were well-correlated to Fe oxide content ($r^2 = 0.99$), and less so to smectite content (0.81) and Mn oxide content (0.60).

Cobalt sorption was more easily interpreted (Fig. 4). Sorption to Tac and Tptpv2 followed a highly nonlinear Freundlich isotherm ($n = 0.57$, 0.55, respectively). Tptpv1 showed a divergence from Freundlich behavior at low concentrations, perhaps due to analytical problems; measured Co concentrations for these points were well under 1 ppb. Neglecting these low-concentration points, sorption to Tptpv1 also followed the Freundlich isotherm ($n = 0.59$). Because of the highly nonlinear nature of Co sorption, fitting a linear isotherm to the data yields K_D values that are strongly concentration dependent, varying over an order of magnitude for each rock type (Table 6). Despite this variability, Co's high degree of sorption is indisputable, with best-fit K_D values ranging from 120 to 1600 g/g.

Nickel, like Mn, showed downward divergence from the Freundlich isotherm at both low and high concentrations (Fig. 4). The high-concentration effect may reflect competition from Co for limited sorption sites. The low-concentration effect cannot be attributed to a Ni background, and may simply reflect analytical difficulties at the low ppb level. By following the same screening process outlined above for Mn, both Freundlich and linear isotherm fits were obtained (Fig. 4). The resulting parameters should be considered quite uncertain. Best fit K_D values fell between those of Mn and Co, ranging from 48 g/g for Tptpv1 to 670 g/g for Tac.

Rhodamine WT sorption results are shown in Fig. 4. Despite some scatter in the data (particularly for the lowest sorbing rock, Tptpv1), the results show a reasonably good fit to a nonlinear Freundlich isotherm, with n ranging from 1.3 to 1.5. Previous detailed studies of rhodamine WT sorption have typically yielded Freundlich exponents less than one (Kasnavia et al., 1999; Sabatini and Austin, 1991); the high n values may be due to peculiarities of the vitric tuff system or the complex tracer mixture matrix. In particular, it has been shown that high KBr concentrations can increase rhodamine WT sorption (Allaire-Leung et al., 1999). Perhaps the LiBr or KI in the tracer mixture also increases rhodamine WT sorption at high concentrations. Overall, rhodamine WT's degree of sorption was quite low, similar to that of Li.

5. Conclusions

Batch measurements of sorption of Np, Pu, and Am onto 3 Busted Butte rocks revealed a wide range in sorption coefficients, with $Np \ll Am$ and $Np \ll Pu$. While both Np and Pu sorption varied with degree of rock alteration (Tptpv1 < Tptpv2 < Tac), Am sorption was similar across the different units, stronger than Pu in some cases, weaker in others. Neptunium and Am sorption parameters were quite similar to those previously reported for similar rocks elsewhere in the Yucca Mountain vicinity. The Pu results showed great variability from rock to rock, with sorption parameters showing a much greater range than typically observed for vitric tuffs.

The tracer sorption measurements described here confirm that the tracer mixtures used in the Busted Butte field experiments include both nonreactive and reactive tracers. The nonreactive tracers (Br^-, I^-, 5 different FBAs, Na fluorescein and "pyridone") did not significantly react with any of the rock types encountered

in the field. The reactive tracers exhibited a very wide range of sorption, spanning approximately 3 orders of magnitude in K_D values. Highly nonlinear sorption behavior of the tracers makes direct comparisons difficult, but results indicate that for concentrations of interest in the field, the metal tracers' degree of sorption is $Li \ll Mn < Ni < Co$. Rhodamine WT, an organic dye, also showed nonlinear sorption to the Busted Butte tuffs, with a degree of sorption roughly similar to that of Li.

The 3 different rock types involved in the Busted Butte field experiments showed varying affinities for both the radionuclides and the reactive tracers. The Calico Hills tuff (Tac), which has the highest smectite, Fe oxide, and Mn oxide content of the 3 (indicating the highest degree of alteration), consistently showed the strongest sorption, while the least altered Tptpv1 layer of the Topopah Springs vitrophyre showed the weakest sorption. The Tptpv2 vitrophyre layer is intermediate both in alteration (as evidenced by clay and oxide content) and degree of sorption.

To a first approximation, the reactive tracers span the same wide range of sorption properties as the radionuclides of concern. Although tracer behavior is not redox-sensitive and thus simpler than radionuclide behavior, Li and Np exhibit similar sorption isotherms, as do Co and Pu.

Acknowledgements

The authors thank Ines Triay and Donald Langmuir for advice on tracer selection, Wendy Soll for support and guidance, and Chris Brink, Steve Chipera, Dale Counce, Schön Levy, Beverly Moore, Gary Parker, and Kyle Roseborrough for experimental and analytical assistance. The manuscript was improved by close reviews by Paul Reimus, Wolfgang Runde, and two anonymous reviewers. This work was supported by the Yucca Mountain Site Characterization Office as part of the Civilian Radioactive Waste Program. This project is managed by the US Department of Energy, Yucca Mountain Site Characterization Program.

References

Allaire-Leung, S.E., Gupta, S.C., Moncrief, J.F., 1999. Dye adsorption in a loam soil as influenced by potassium bromide. J. Environ. Qual. 28, 1831–1837.

Anghel, I., Turin, H.J., Reimus, P.W., 2002. Lithium sorption to yucca mountain tuffs. Appl. Geochem.

Atkinson, T.C., Bukowiecki, A.A., 2000. Sorption of fluorobenzoic acids on peat and kaolinite. In: Dassargues, A. (Ed.), Tracers and Modelling in Hydrogeology. IAHS Publication 262, International Association of Hydrological Sciences, Wallingford, UK, pp. 187–194.

Bowman, R.S., Urquhart, N.S., O'Connor, G.A., 1984. Statistical evaluation of sorption isotherm data. Soil Sci. 137, 360–369.

Bussod, G.Y., Coen, K. and Eckhardt, R.C., 1998. LA Testing Status Report: Busted Butte Unsaturated Zone Transport Test. Yucca Mountain Site Characterization Project Milestone SPU85M4. Los Alamos National Laboratory.

Farnham, I.M., Meigs, L.C., Dominguez, M.E., Lindley, K., Daniels, J.M. and Stetzenbach, K.J., 2000. Appendix H: evaluation of tracers used for the WIPP tracer tests. In: L.C. Meigs, R.L. Beauheim and T.L. Jones (Eds.), Interpretations of Tracer Tests Performed in the Culebra Dolomite at the Waste Isolation Pilot Plant Site. Sandia National Laboratories Report SAND97–3109, pp. 273–289.

Gambrell, R.P., 1996. Manganese. In: Sparks, D.L., Page, A.L., Helmke, P.A., Loeppert, R.H., Soltanpour, P.N., Tabatabai, M.A., Johnson, C.T., Sumner, M.E. (Eds.), Methods of Soil Analysis. Part 3. Chemical Methods. Soil Science Society of America and American Society of Agronomy, Madison, WI, pp. 665–682.

Geldon, A.L., Umari, A.M.A., Fahy, M.F., Earle, J.D., Gemmell, J.M. and Darnell, J., 1997. Results of Hydraulic and Conservative Tracer Tests in Miocene Tuffaceous Rocks at the C-Hole Complex, 1995–1997, Yucca Mountain, Nye County, Nevada. Yucca Mountain Site Characterization Project Milestone SP23PM3, U.S. Geological Survey.

Kasnavia, T., Vu, D., Sabatini, D.A., 1999. Fluorescent dye and media properties affecting sorption and tracer selection. Ground Water 37, 376–381.

Kearney, M.L., Wolfsberg, L.E., Groffman, A.R., Jones, C.L., Turin, H.J., 2000. Solubility of rare earth elements and transition metals as a function of increasing pH during unsaturated-zone transport tests at Busted Butte, Nevada. Geol. Soc. Am. Abst. 32, A-209.

Loeppert, R.H., Inskeep, W.P., 1996. Iron. In: Sparks, D.L., Page, A.L., Helmke, P.A., Loeppert, R.H., Soltanpour, P.N., Tabatabai, M.A., Johnson, C.T., Sumner, M.E. (Eds.), Methods of Soil Analysis. Part 3. Chemical Methods. Soil Science Society of America and American Society of Agronomy, Madison, WI, pp. 639–664.

Müller, J., 2000. Large-scale field experiments on the mobility of heavy metals (As, Cd, Co, Cr, Cu, Hg, Ni, Pb, Sb, Se, Zn) in groundwater. In: Dassargues, A. (Ed.), Tracers and Modelling in Hydrogeology. IAHS Publication 262. International Association of Hydrological Sciences, Wallingford, UK, pp. 135–140.

Nelson, D.A., Bush, J.H., Beckett, J.R., Lenz, D.M., Rowe, D.W., 1989. Use of fluorescent 1;3-disubstituted 2(1H) pyridones for environmental-analysis. ACS Sympo. Series 383, pp. 206–227.

Reimus, P.W., Haga, M.J., Callahan, T., Anghel, I., Turin, H.J. and Counce, D., 1998. C-Holes Update Report: Reinterpretation of the Reactive Tracer Test in the Bullfrog Tuff and Results of Laboratory Testing. Yucca Mountain Site Characterization Project Milestone SP32E2M4SZ Los Alamos National Laboratory.

Reimus, P.W., Adams, A., Haga, M.J., Humphrey, A., Callahan, T., Anghel, I. and Counce, D., 1999. Results and Interpretation of Hydraulic and Tracer Testing in the Prow Pass Tuff at the C-Holes. Yucca Mountain Site Characterization Project Milestone SP32E7M4. Los Alamos National Laboratory.

Sabatini, D.A., Austin, T.A., 1991. Characteristics of rhodamine WT and fluorescein as adsorbing ground-water tracers. Ground Water 29, 341–349.

Schwertmann, U., Taylor, R.M., 1989. Iron oxides. In: Dixon, J.B., Weed, S.B. (Eds.), Minerals in Soil Environments. Soil Science Society of America, Madison, WI, pp. 145–180.

Triay, I.R., Meijer, A., Conca, J.L., Kung, K.S., Rundberg, R.S., Strietelmeier, B.A., Tait, C.D., Clark, D.L., Neu, M.P. and Hobart, D.E., 1997. Summary and Synthesis Report on Radionuclide Retardation for the Yucca Mountain Site Characterization Project. Yucca Mountain Site Characterization Project Milestone 3784M. Los Alamos National Laboratory.